Engineered Science
DOI: https://dx.doi.org/10.30919/es1866

Downhole Oil-Water Segregation in Production Wells: Review, Design, Simulation and Field Trials

Marat Sagyndikov,[1,2,*] Iskander Gussenov,[1,3] Alexey Shakhvorostov,[1] Yerzhan Melis,[1] Ilshat Salimgarayev,[1,2] Batyrzhan Shilanbayev,[2,3] Reza Khoramian[4] and Zhalgas Imanbayev[1,5]

Abstract

Excessive water production increases lifting costs and shortens well life, yet existing control methods remain inadequate-chemical treatments are short-lived, mechanical systems costly, and cyclic operations disruptive. To overcome these issues, this study presents a Downhole Fluid Segregation workflow that exploits gravity-driven phase separation in the wellbore to selectively produce oil while retaining excess water in the reservoir. Calculations showed single oil blobs rose through a water column within 1-16h, with transit time decreasing as droplet size increased. Analytical scaling indicated that stabilization time increases sharply with reservoir thickness but decreases with vertical permeability. For instance, for a 13-m-thick reservoir with a vertical permeability of 400 mD, full rebalancing required 193 days. Reservoir simulations of a 15-month shut-in increased oil saturation in upper intervals from ~0.2-0.4 up to ~0.6. Restarting production at moderate rates provided the best balance between oil recovery and water control, while high rates caused early water breakthrough. Field pilots in Western Kazakhstan confirmed feasibility: watercut fell to <1% even in a well producing 8,500cP oil, while medium-viscosity wells showed increased oil output and watercut decline from 95-98% to <1%. Limitations include fractures, low kv, and fluid-stability constraints. Future work targets full automation and multiwell pilot verification.

Keywords: Water production; Watercut control; Downhole fluid segregation; Wellbore gravity oil–water separation; Field pilots; Enhanced oil recovery (EOR).
Received: 18 September 2025; Revised: 27 October 2025; Accepted: 06 November 2025
Article Type: Review article.

1. Introduction

High water production, expressed as the water cut (WC), remains one of the most persistent challenges in oilfield operations,[1,2] directly affecting both economic and technical performance.[3] Increasing WC sharply elevates lifting and treatment costs, reducing profitability and shortening well life.[4] In addition to its economic impact, excessive water production accelerates corrosion in downhole and surface facilities, particularly in CO2-bearing environments where corrosion rates of carbon and tube steels rise with water fraction and temperature.[5-7]

Several strategies have been developed to mitigate this problem, generally grouped into chemical, mechanical,[8] and operational methods. Chemical conformance treatments, principally polymer and cross-linked-gel systems, aim to block high-permeability channels and improve sweep efficiency.[9-13] Laboratory and field applications have shown that such gels can temporarily reduce permeability contrast and lower WC; however, they often degrade under elevated temperature or salinity, have long dissolution times, and may cause irreversible formation damage.[14-16] Mechanical technologies, such as Downhole Oil–Water Separation (DOWS) systems, attempt to physically separate oil and water within the wellbore and reinject the separated water into adjacent strata through dual completions. Field trials in Alliance (Canada) and La-Victoria (Argentina),[17-19] and later applications in Lacq Supérieur (France), the North Sea, China, and the USA,[20-23] confirmed the technical feasibility of DOWS. Nevertheless, corrosion, scaling, injectivity decline, and high equipment cost limited widespread adoption.[24,25] Operational approaches, including Cyclic Production Schemes (CPS), regulate water inflow through intermittent pumping or controlled shut-in cycles. Examples include the

[1]*Institute of Polymer Materials and Technology, microdistrict "Atyrau 1", 3/1, Almaty, 050019, Kazakhstan*
[2]*Researching and Development LLP, microdistrict 29, b.4, Aktau, 130000, Kazakhstan*
[3]*Satbayev University, 22a Satpaev Street, Almaty, 050013, Kazakhstan*

Leninogorskneft field, where intermittent operation reduced energy use and extended equipment life;[26] the Tananik well, where mean time between repairs increased from 45 to 832 days;[27] and the CQ1 well in China, which achieved higher system efficiency and lower power consumption under intelligent on/off control.[28] Modeling by Al-Mutairi *et al*. (2008)[29] and subsequent patents[30] confirmed the potential of cyclic operation but emphasized its dependence on reservoir heterogeneity and the loss of production during downtime.

Another technology which should be mentioned is Downhole Water Sink (DWS). The concept was introduced by Wojtanowicz *et al*. (1991)[31] as a dual-completion method to control water coning by producing water from below the oil–water contact. Subsequent work demonstrated that DWS can accelerate recovery up to five-fold and increase oil recovery by 30–70% compared with conventional completions,[32] though at the expense of higher total water production.

Recent studies extended the method to hybrid Gas-Downhole Water Sink-Assisted Gravity Drainage (GDWS-AGD) and Triple-Completion GDWS-AGD (TC-GDWS-AGD) processes.[33-36] These configurations integrate gas injection and water drainage to enhance recovery and reduce water cut in aquifer-driven reservoirs, achieving up to 82% oil recovery and water cuts as low as 5%. Optimization studies demonstrated that triple-completion designs maximize oil production with fewer wells and lower water handling.

Further modeling by Zeynolabedini and Assareh (2021)[37] highlighted the sensitivity of DWS performance to anisotropy, drainage rate, and completion length.

A concise comparison of above-described classes of water-control methods, including their operating principles, configurations, advantages, and limitations, is presented in Table 1.

Despite significant progress, existing methods fail to provide a sustainable and continuous solution. Chemical treatments are short-lived and environmentally sensitive; mechanical systems are expensive and complex; and cyclic operation sacrifices production time. To overcome these limitations, this study introduces a Downhole Fluid Segregation (DFS) technique that exploits natural gravitational separation of oil and water within the wellbore. The method repositions the pump intake above the stabilized oil–water boundary (OWB) and employs automated surface control to selectively withdraw oil while suppressing water inflow. By eliminating chemical additives, water reinjection, and prolonged shut-ins, DFS offers a continuous, low-cost, and environmentally sustainable alternative for managing high-WC wells. The overall workflow of the study—from conceptual development through laboratory validation, modeling, and field testing—is summarized in Fig. S1 (ref. to Supporting information).

[4]*School of Mining and Geosciences, Nazarbayev University, 53 Kabanbay Batyr Avenue, Astana, 010000, Kazakhstan*
[5]*Republican Public Association (RPA) "Veterans of the Oil and Gas Complex" (VOGC), 19 Kabanbay Batyr Avenue, Astana, 010000, Kazakhstan*
[*]*Email:* sagyndikov.marat.s@gmail.com (Marat Sagyndikov)

2. Materials and methods

This study integrates field data analysis, laboratory experiments, analytical modeling, and numerical simulation. The methodological workflow consists of four primary components: (i) reference well characterization, (ii) fluid and droplet-scale segregation analysis, (iii) reservoir-scale analytical calculations, and (iv) field-scale numerical simulation, supporting the results of pilot trials.

The Supporting Information section presents the configuration of the surface and wellbore equipment, along with the workflow proposed for field implementation of the technology (Fig.S2-S4).

2.1 Reference reservoir and fluid characterization

To establish a quantitative framework and define representative boundary conditions for subsequent analyses, a high-water-cut producer (Well A) from the Kalamkas field was selected as a reference case. This well typifies mature, water-invaded sandstone reservoirs in western Kazakhstan and provides reliable static and dynamic data for validating droplet-rise behavior, laboratory column tests, and reservoir-scale equilibration modeling. The key parameters are summarized in Table 2.

In the following sections, a quantitative framework based on a high–water-cut reference producer (Well A, Kalamkas) is established to parameterize laboratory, analytical, and numerical work. Analytical and numerical descriptions of multiphase segregation in open conduits and porous media are well documented in the literature.[45,46]

Crude oils were sampled and stored under standard protocols. Degassed oils viscosities were measured at temperature range 25-45 ºC and shear rates up to 100 s^{-1} using RheolabQC (AntonPaar) viscometer. Rheological measurements on crude samples from the Kalamkas (Fig. 1a) and Karazhanbas (Fig. 1b) fields revealed pronounced non-Newtonian shear-thinning behavior, with viscosity decreasing as shear rate increased due to the influence of dispersed asphaltenes and waxes. Representative dynamic viscosities were determined as 29 cP at 45 °C for Kalamkas and 635 cP at 25 °C for Karazhanbas, each with an uncertainty of ± 1 cP. This viscosity contrast

Table 1: Comparison of major water-cut-control technologies and the proposed Downhole Fluid Segregation (DFS) method.

Technology	Core Principle	Typical Configuration	Main Advantages	Key Limitations	References
Gels	Reduce permeability contrast by blocking high-permeability zones using cross-linked-gel systems.	Gelant injection via tubing into production or injection intervals.	Simple deployment; short-term WC reduction.	Thermal/salinity degradation; possible formation damage; high chemical cost; environmental concerns.	[16, 38-41]
Downhole Oil–Water Separation (DOWS)	Separate oil and water in the wellbore and reinject produced water into a nearby formation through a dual completion.	Hydrocyclone separator combined with an Electric Submersible Pump (ESP).	Downhole water disposal; reduced surface handling; up to 50 % lower power use.	High installation cost (USD 120–300 k); injectivity decline; corrosion and scaling; large-casing requirement (≥ 5½″).	[17-25,42]
Cyclic Production Schemes (CPS)	Alternate pumping and shut-in periods to equalize formation pressures and reduce water inflow on restart.	Intermittent or intelligent pumping systems with real-time control.	Lower energy use (~15–30 %); longer equipment life; improved oil quality.	Requires downtime; response varies with heterogeneity; limited cumulative recovery.	[27-30,43,44]
Downhole Water Sink (DWS) and Gas-Downhole Water Sink-Assisted Gravity Drainage (GDWS-AGD)	Controlled drainage of water below the oil–water contact to suppress water coning and enhance oil drainage; in hybrid forms, combined with gas injection for pressure support and gravity segregation.	Dual or triple completions: upper horizontal section for oil production, lower for water drainage, and vertical or upper completion for gas injection, separated by packers.	Reduces water cut, delays water breakthrough, increases oil recovery (up to 30–70%).	High completion cost, complex well design.	[31, 33-37]
Proposed Downhole Fluid Segregation (DFS)	Utilize natural gravitational segregation of oil and water within the wellbore; selectively pump from the oil layer above the stabilized oil–water boundary (OWB).	Repositioned pump intake + surface automation with real-time WC monitoring and automatic shut-off.	No chemicals or reinjection; continuous low-rate production; automated WC control; lower cost and energy use.	Requires sufficient vertical permeability; sensitive to fractures and cold-flow conditions.	This study (Sections 2–4).

Table 2: Reference dataset for production Well A (Kalamkas), 1 Jan 2024.

Parameter	Value
Production start date	May 1984
Formation	J-1 / Sandstone
Cumulative oil production (t)	118,099
Cumulative water production (t)	617,684
Depletion of recoverable reserves (f_w = 98 %)	83.7 %
Current oil rate (t·day^{-1})	4.0
Current water rate (t·day^{-1})	57.5
Water cut (WC, %)	93.6
Lift system	Sucker-rod pump
Dynamic level in annulus (m)	100
Fluid level above pump (m)	500
Calculated bottomhole pressure (atm)	69
Estimated average reservoir pressure (atm)	92

Parameter	Value
Perforation interval (m)	851–865
Oil-saturated thickness (m)	13
Average permeability (mD)	409
Average porosity (%)	30.6
Average oil saturation (%)	75.9
Average water saturation (%)	19.6

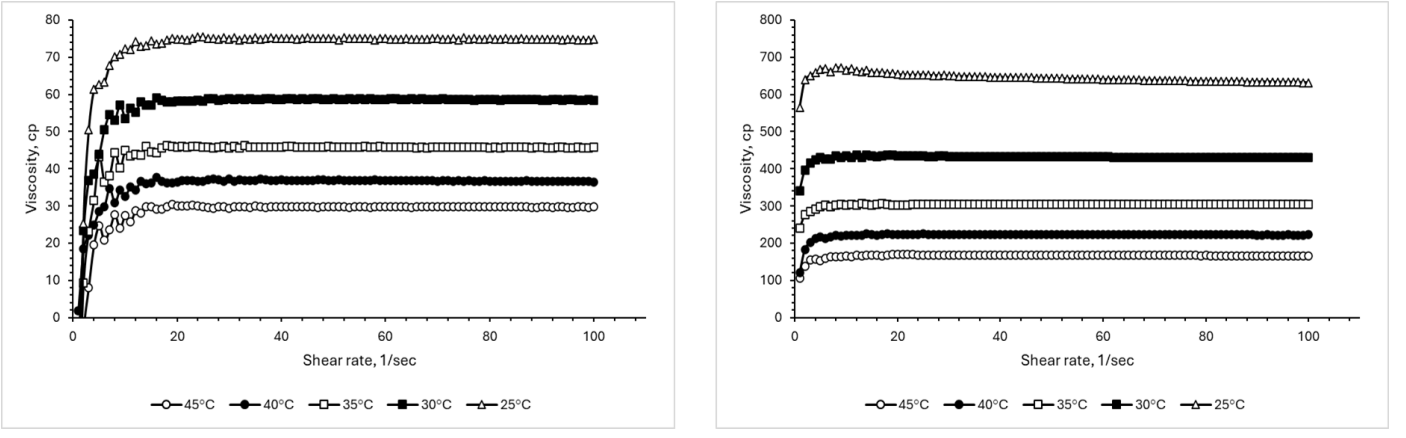

Fig.1: Rheological behavior of crude oils used in gravity-segregation analysis: (a) Kalamkas crude at 45 °C; (b) Karazhanbas crude at 25 °C. Measurement uncertainty for both datasets is ± 1 cP.

spanning more than an order of magnitude—defines the mobility range relevant to buoyancy-driven separation: Kalamkas represents a moderately mobile system, whereas Karazhanbas exemplifies the low-mobility limit typical of heavy-oil reservoirs. These rheological inputs were applied in the Hadamard–Rybczynski calculations and numerical simulations described below.

2.2 Droplet ascent experiment

A transparent acrylic column (height = 0.30 m, inner diameter = 0.05 m) filled with formation-analog water at 20 °C was used to investigate oil-droplet rise dynamics in quiescent conditions (Fig. 2). Degassed Kalamkas oil was injected through a capillary nozzle at the base of the column, and the ascent of individual droplets was recorded using a high-speed digital camera to provide empirical input for the numerical model.

2.3 Numerical simulation of droplet rise

To complement the laboratory observations, a transient two-phase Level Set simulation was performed in COMSOL Multiphysics to reproduce the ascent of oil droplets in water and quantify velocity–shape evolution under laminar conditions. The model geometry was 2D axisymmetric (45 cm height × 5 cm width), initialized with an oil droplet near the base of a quiescent water column. Physical properties (density, viscosity, and interfacial tension) were set to match the experimentally measured values for the Kalamkas crude. Boundary conditions included no-slip walls, axial symmetry, and a pressure outlet at the top. Hydrostatic equilibrium was imposed prior to release, and the simulation started with zero velocity in both phases. The Continuum Surface Force (CSF) approach was used to represent interfacial tension, while the Level Set method captured the evolving oil–water interface with adaptive mesh refinement (11,591 elements; 11,545 triangular + 46 quadrilateral cells). Fig. 3 illustrates the computational mesh, showing high resolution near the interface to ensure accurate curvature tracking. The model solved the incompressible Navier–Stokes equations coupled with the Level Set transport Eq. (1-3)[47]:

$$\rho(\partial u/\partial t+u\cdot\nabla u)=-\nabla p+\mu\nabla 2u+Fst+\rho g \quad (1)$$

$$\nabla\cdot u=0 \quad (2)$$

$$\gamma\nabla\cdot(\varepsilon\nabla\phi-\phi(1-\phi)\nabla\phi/|\nabla\phi|)=0 \quad (3)$$

where u is velocity, p pressure, ρ and μ the phase-dependent density and viscosity, Fst the surface-tension force, and ϕ the Level Set function. Parameters γ and ε control interface reinitialization and thickness, respectively.

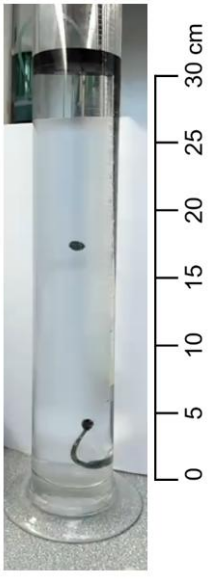

Fig. 2: Experimental setup used to measure the ascent velocity of Kalamkas oil droplets in water.

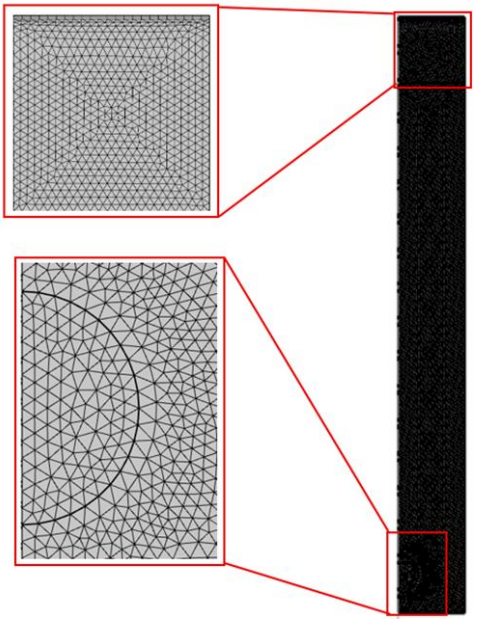

Fig. 3: Structured 2D axisymmetric mesh highlighting refinement around the oil droplet for accurate interface representation.

2.4 Analytical estimation of droplet transport

The terminal rise velocity of a clean, nearly spherical droplet at low Reynolds number was approximated by the Hadamard–Rybczynski expression Eq. (4)[46]:

$$U_{\infty} = \frac{2}{9} \cdot \frac{a^2 g(\rho' - \rho'')}{\mu} \frac{3\mu' + 3\mu}{3\mu' + 2\mu} \qquad (4)$$

where U_{∞} is velocity of movement (m·s^{-1}), α droplet radius (m), g gravity (m·s^{-2}), ρ' and ρ'' are water and oil densities (kg·m^{-3}), μ and μ' are the outer (water) and inner (oil) viscosities (mPa·s).

This relation idealizes several conditions: (1) Re $\ll$ 1; (2) perfect sphericity; (3) infinite, quiescent medium; (4) Newtonian fluids; and (5) a clean, mobile interface.

In wellbores, these assumptions are partly violated. For a 10 mm Kalamkas droplet (v = 0.033 m/s, Re = 330), inertial forces and wall confinement increase drag, while droplet deformation and shear-thinning rheology modify flow behavior. Moreover, interfacial films from asphaltenes can immobilize the surface, reducing internal circulation. Despite these deviations, the Hadamard–Rybczynski model remains a practical first-order approximation, providing an upper bound for rise velocity and a useful baseline for interpreting segregation dynamics.

2.5 Reservoir-scale capillary–gravity re-equilibration estimations

Vertical fluid redistribution during shut-in was evaluated using the analytical model of Bakhtiy *et al.* (2015),[45] which combines buoyancy and capillary-pressure effects (Eq. 5–11).

The equilibration time t_e is given by Eq. (5-6)[45]:

$$t_e=(\sqrt{h}+\sqrt{H-h})^2/C_t \quad (5)$$

$$C_t=\frac{-k_z\gamma}{0.5(\mu_w+\mu_o)\varphi H} \quad (6)$$

Here H - reservoir thickness;
h - height of the oil–water contact;
k_z - vertical permeability;
$\gamma=(\rho_o-\rho_w)g$ - buoyancy term;
ρ_w and ρ_o - densities of water and oil;
μ_w and μ_o - viscosities of water and oil;
ϕ - porosity;
and g - gravitational acceleration.

Vertical variations in saturation can be expressed through a capillary-pressure closure Eq. (7-9)[45]:

$$P_c(x, s_w)=\varphi(x)J(S_w) \quad (7)$$

$$\varphi(x)=\delta\cos\theta\sqrt{\frac{\phi}{k}} \quad (8)$$

$$J(S_w)=(1-S_w)^2 \quad (9)$$

Here P_c – capillary pressure;
x – vertical coordinate;
S_w – water saturation;
$\varphi(x)$ – maximal capillary pressure;
ϕ - the porosity;
k - vertical permeability;
$J(S_w)$ - Leverett j-function;
δ – interfacial tension;
θ – contact angle.

Using a representative capillary-pressure profile[45] Eq. (10):

$$\varphi(x)= 0.0001x^2 - 0.404x + 408.5 \text{ MPa} \quad (10)$$

where x denotes the depth of the oil–water contact (OWC), the corresponding oil-saturation distribution becomes Eq. (11)[45]:

$$S_o(x)=\sqrt{\frac{-0.00196(x-20115)}{0.0001x^2-0.404x+408.5}} \quad (11)$$

This formulation links capillary pressure and vertical saturation gradients to measurable rock and fluid properties such as permeability, viscosity, and density contrast.

In these calculations the formation thickness and vertical permeability were varied parametrically to quantify their influence on equilibration time (Fig. 7). Reference-well parameters from Kalamkas were applied to estimate required shut-in durations for practical segregation.

2.6 Field-scale numerical reservoir simulation

To complement the analytical predictions and field observations, a numerical reservoir model was constructed to simulate the long-term redistribution of oil and water during well shut-in and to identify the optimal restart rate that minimizes water cut while maximizing cumulative oil recovery. Simulations were performed using tNavigator, applying the compositional two-phase flow formulation with adaptive time-stepping and pressure–saturation coupling.

2.6.1 Model setup and parameters

A representative sector model was extracted from the Nuraly oil field surrounding production Well No. 402. The sector encompassed an area of 500 m radius, discretized into a 50 × 50 × 0.25 m grid (512 583 active cells) to resolve vertical segregation with high fidelity. Constant-pressure boundaries were imposed at the model periphery, while peripheral source–sink terms were adjusted using productivity-index tables. Initial conditions and rock–fluid properties were adopted from field measurements (Table 3). The model considered isotropic porosity but included anisotropic permeability with a k_h/k_v=10 ratio to reflect layered reservoir heterogeneity. Adaptive time-stepping satisfied the Courant stability criterion, with residuals limited to 10–3.

Table 3: Reservoir model input parameters.

Parameter	Symbol	Value
Average effective porosity	(ϕ)	0.158
Horizontal permeability (mD)	(k_h)	124
Vertical permeability (mD)	(k_v)	12
Anisotropy ratio	(k_h/k_v)	10
Initial reservoir pressure (MPa)	(P_i)	16.2
Reservoir temperature (°C)	(T)	57
Oil viscosity (cP)	(μ_o)	0.52
Water viscosity (cP)	(μ_w)	0.58

2.6.2 Simulation procedure

Three sequential stages were modeled:

Stage 1 – Shut-in phase (June 2023 – September 2024): production was halted to allow gravitational segregation and re-equilibration of fluids.

Stage 2 – Restart phase: production resumed at constant rates

of 5, 10, 15, and 25 $m^3 \cdot day^{-1}$ to evaluate restart performance.

Stage 3 – Partial-perforation test: only half of the original interval was opened to assess potential flow isolation strategies.

The corresponding simulation results and their implications for managing high-water-cut well performance are summarized below.

3. Results and discussion

3.1 Wellbore-scale fluid segregation: estimating oil-droplet rise velocities and wellbore separation times

The transparent acrylic column experiments designed to investigate oil-droplet rise dynamics in quiescent conditions showed that stable oil droplets formed within a 5–20 mm size range, with a typical horizontal diameter of approximately 13 mm and a thickness of 3 mm. Droplets smaller than 5 mm could not be generated due to interfacial-tension constraints, while those larger than 20 mm disintegrated under their own weight. A 13 mm droplet ascended 0.3 m in 9.2 ± 0.05 s, establishing a representative rise velocity under laminar conditions. These experimental observations confirm the feasibility of buoyancy-driven segregation for moderately viscous oils and provide the physical parameters required for subsequent modeling. Moreover, the static experimental conditions are close to those in a wellbore during the shut-in period, when turbulent flow is absent and gravity-driven rise and coalescence of oil globules prevail. Therefore, the observed droplet size range represents the key segregation phase and provides the data necessary to calculate rise velocities and determine the optimal shut-in time for effective phase separation in the field.

The 2D Level Set simulation reproduced the experimentally observed ascent of oil droplets with high accuracy. As shown in Fig. 4, the model captured both droplet deformation and rise velocity consistent with laboratory results. The droplet evolved from a nearly circular shape at initialization to a semi-elliptical geometry as buoyancy overcame viscous resistance. Progressive elongation under shear and drag became evident in intermediate frames, followed by steady ascent to the column top after approximately 9 s, closely matching the experimental transit time of 9.2 s. To visualize this process more intuitively, the same axisymmetric dataset was revolved to generate a 3D reconstruction (Fig. 5). The three-dimensional sequence highlights the droplet's vertical trajectory and morphological evolution—from initial detachment at the base to full stabilization near the free surface—demonstrating smooth interface tracking and stable numerical performance. The close correspondence between the 2D simulation, 3D reconstruction, and laboratory measurements validates the model's capability to represent buoyancy-driven segregation under laminar flow conditions.

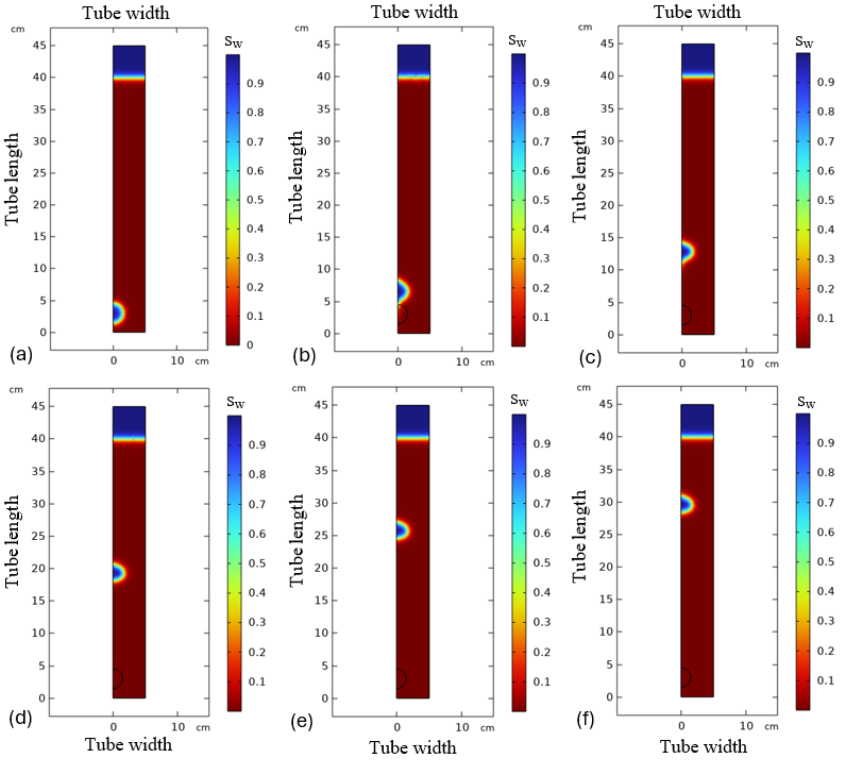

Fig. 4: Simulation snapshots of oil droplet rise in still water (2D, Level Set model). The oil fraction is represented in color (red = oil, blue = water). Frames (a–f) capture the droplet's motion from the initial bottom location to time steps at 2, 4, 6, 8, and 9 s.

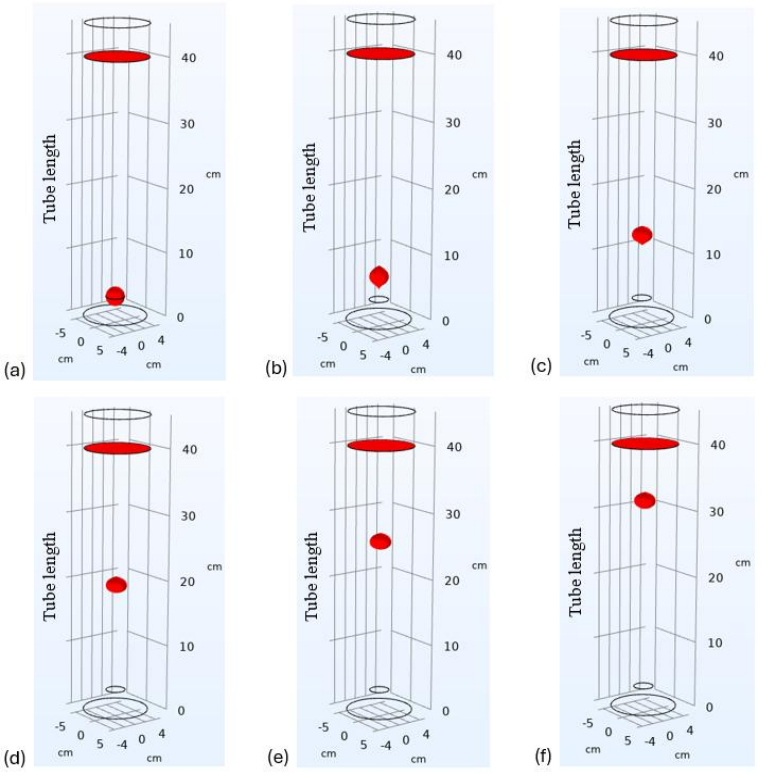

Fig. 5: 3D visualization of the oil droplet's rise, derived from axisymmetric model data. Subfigures (a–f) represent snapshots at 0 s, 2 s, 4 s, 6 s, 8 s, and 9 s, capturing changes in position and morphology during upward motion.

While the numerical model reproduces laboratory-scale behavior, field applications require first-order estimates of how rapidly droplets can traverse hundreds of meters of static brine in a wellbore. This scaling was achieved using the Hadamard–Rybczynski formulation and field-specific inputs (Table 4). As a results, the velocity–diameter curves were generated for Kalamkas (Fig. 6a) and Karazhanbas (Fig. 6b). Illustratively, a 5 mm droplet at Kalamkas (45 °C, μ' 29 cP) rises at 0.55 m·min^{-1}, crossing 500 m in ~15 h; at Karazhanbas (25 °C, μ' 635 cP) it rises at 0.22 m·min^{-1}, crossing 250 m in ~16 h. Thus, in a quiescent wellbore, individual oil blobs can traverse long columns within hours to a day for the tested fluids and sizes.

Table 4: Inputs for Hadamard–Rybczynski droplet-rise calculations in the Kalamkas and Karazhanbas fields.

Parameter	Symbol	Kalamkas	Karazhanbas
Oil droplet diameter (mm)	(d)	5–20	5–20
Gravity (m·s^{-2})	(g)	9.81	9.81
Water density (kg·m^{-3})	(ρ')	1,000	1,000
Degassed oil density (kg·m^{-3})	(ρ'')	900	940
Outer-phase viscosity (mPa·s)	(μ)	1	1
Oil viscosity (mPa·s)	(μ')	29(45 °C)	635 (25 °C)
Column height (m)	(H)	500	250
Temperature (°C)	(T)	45	25

3.2 Reservoir-scale fluid segregation: estimating the effects of reservoir thickness and vertical permeability

Analytical evaluation highlights two dominant controls on equilibration time—formation thickness and vertical permeability. As shown in Fig. 7a–b, the time required for gravitational rebalancing increases sharply with layer thickness but decreases with higher vertical permeability. Doubling H extended t_e by roughly 24 times, whereas increasing k_z from 0.1 to 1 Darcy shortened equilibration from 1,241 to 124 days. Applying this model to the Kalamkas well (H=13 m, k_z = 0.4 D, ϕ=0.31 from Table 2) yields an equilibration time of ~193 days, indicating that multi-month shut-in periods are sufficient for near-complete capillary–gravity segregation. This order-of-magnitude consistency with field pilots demonstrates that reservoir-scale segregation under realistic permeability–thickness conditions can occur within operationally practical timeframes.

These analytical results confirm that gravity-driven fluid re-equilibration can occur within several months in permeable formations, providing a realistic physical basis for the observed field performance of DFS. However, to capture the coupled effects of permeability anisotropy, reservoir depletion, and dynamic restart conditions, a numerical approach is required. The following section therefore employs a compositional reservoir model to quantify fluid redistribution during shut-in and evaluate the optimal restart strategy for minimizing water cut while maximizing oil recovery.

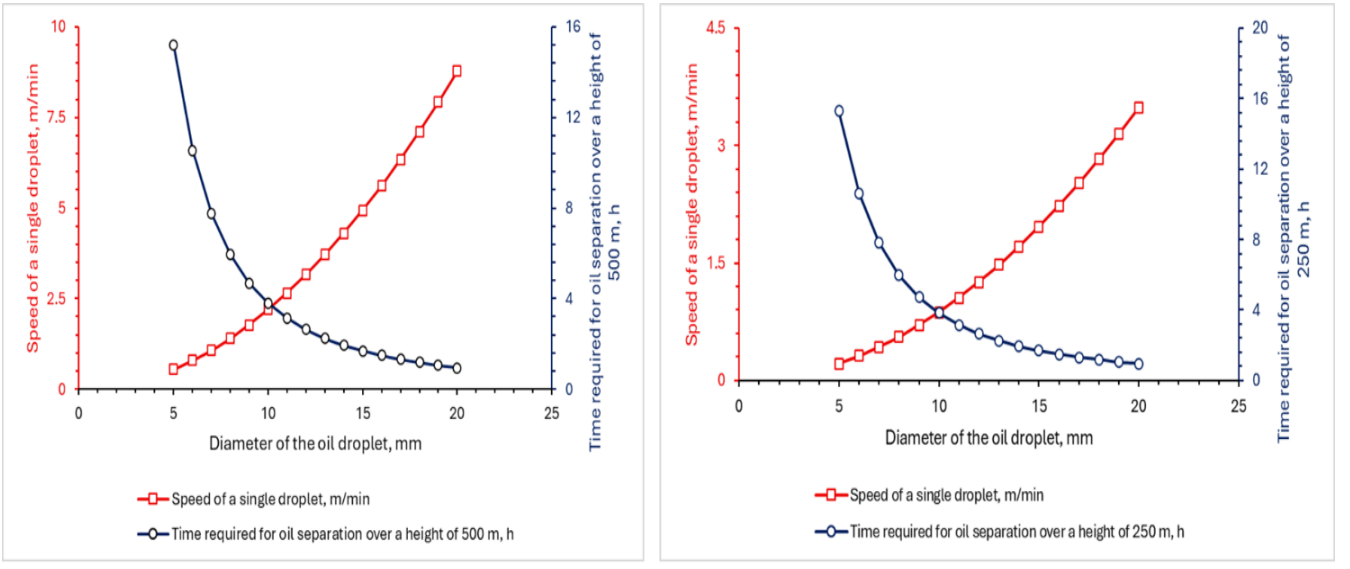

Fig. 6: Calculated rise velocities of oil droplets with varying diameters based on the Hadamard–Rybczynski model: (a) Kalamkas field at 45 °C; (b) Karazhanbas field at 25 °C.

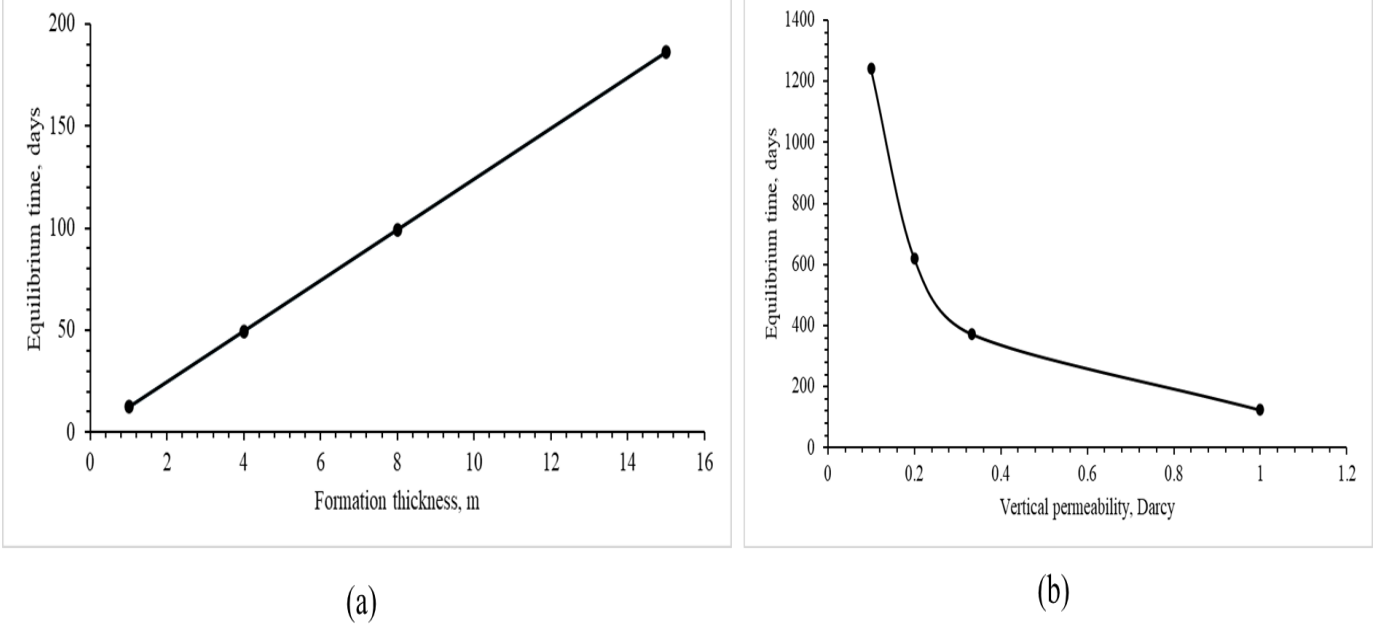

Fig. 7: Analytical relationships for capillary–gravity equilibration: (a) Effect of formation thickness on equilibration time; (b) Effect of vertical permeability on equilibration time.

3.3 Field-scale numerical simulation

3.3.1 Simulation of shut-in–induced oil segregation

As a first step, the numerical model was used to demonstrate the effect of the shut-in period (June 2023 – September 2024) on gravitational segregation and fluid re-equilibration. The spatial evolution of oil saturation during the shutdown and restart is illustrated in Fig. 8. Before production (Fig. 8a), oil saturation was uniformly high across the pay zone. By June 2023 (Fig. 8b), prolonged depletion had depressed the oil–water contact, causing nearly complete water invasion in the lower interval. After approximately 15 months of shut-in (Fig. 8c), gravitational segregation re-established an oil column above the oil–water contact (OWC). Oil saturation in the upper perforation interval (1,537 m) increased from 0.25–0.45 to approximately 0.6, reflecting gravity-driven redistribution. In addition, the model indicates that the oil–water contact stabilized near 1,541 m, with residual movement of less than 0.2 m·month^{-1}. The bottomhole pressure increased from 93 to 96 atm, confirming the establishment of static equilibrium.

The right-hand panel (Fig. 8d) presents a geostatistical

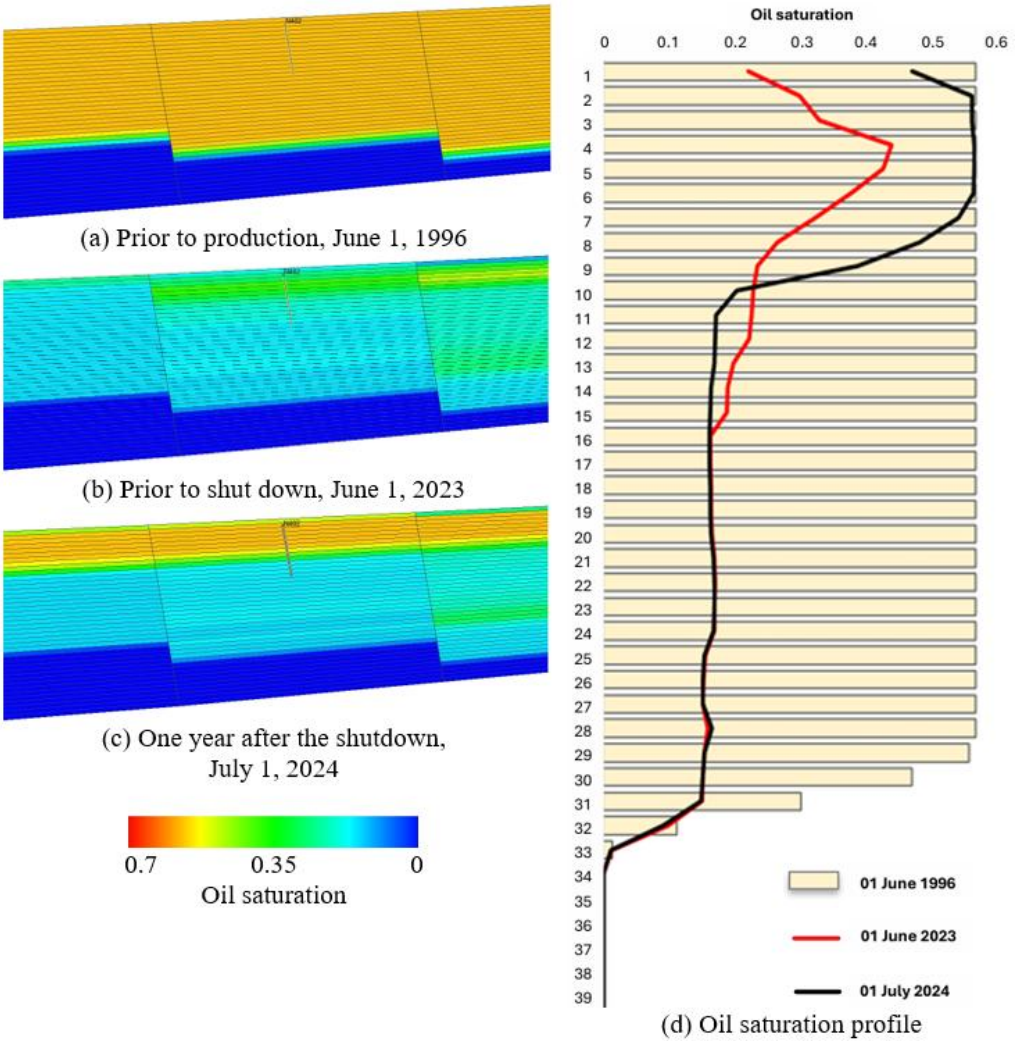

Fig. 8: Evolution of oil saturation during production and shut-in for the modeled well. Panels (a–c) show progressive redistribution of fluids—from initial uniform saturation to water invasion and finally gravity-driven oil restoration after one year of shut-in. Panel (d) presents a geostatistical cross-section along the well trajectory, highlighting increased oil saturation (0.25–0.45 → ~0.6) in the upper perforation interval near 1,537 m due to capillary–gravity re-equilibration.

section along the well trajectory, confirming the upward shift of the oil-rich zone and matching the capillary–gravity re-equilibration trends predicted analytically.

3.3.2 Restart-rate optimization

Restart simulations were performed to evaluate the effect of constant flow rates (5, 10, 15, and 25 $m^3 \cdot day^{-1}$) on post-shutdown performance. The key outputs—maximum and time-dependent water cut (WC) and cumulative oil and water production—are summarized in Table 5. High restart rates (≥ 20 $m^3 \cdot day^{-1}$) induced rapid water-cone reformation, leading to early breakthrough and sustained high WC. Conversely, low rates (5–10 $m^3 \cdot day^{-1}$) minimized water inflow but limited total recovery due to insufficient drawdown. The intermediate case of 15 $m^3 \cdot day^{-1}$ achieved the optimal balance: WC remained below 31 % during the first six months while cumulative oil recovery was maximized. This behavior reflects the sensitivity of DFS performance to the balance between gravitational segregation and viscous forces controlling the oil–water interface.

The corresponding production behavior under different restart rates is shown in Fig. 9. As can be seen, excessive drawdown (≥ 20 m3·day⁻1) rapidly regenerated a water cone, driving WC above 60 % within six months. In contrast, moderate restart at 15 m3·day⁻1 stabilized the interface and achieved the highest cumulative oil recovery, whereas lower rates (5–10 m3·day⁻1) produced minimal WC but suboptimal oil output. These results demonstrate that controlled drawdown following sufficient shut-in facilitates sustainable selective oil production and delayed water breakthrough—confirming the practical advantage of the DFS approach for long-term high-WC well management.

Table 5: Numerical simulation results for different restart flow rates.

Parameter	Flow Rate			
	5·day^{-1}	10 m^3·day^{-1}	15 m^3·day^{-1}	25 m^3·day^{-1}
Maximum WC (%)	49	55	59	90
WC after 60 days (%)	15	18	22	37
WC after 180 days (%)	20	25	31	62
Cumulative oil (× 10^3 m^3)	4.6	8.3	11.4	8.1
Cumulative water (× 10^3 m^3)	3.1	3.8	3.8	3.8
Description	Lowest water cut, low oil rate	Acceptable, not optimal	Optimal balance	Rapid water-cone reformation

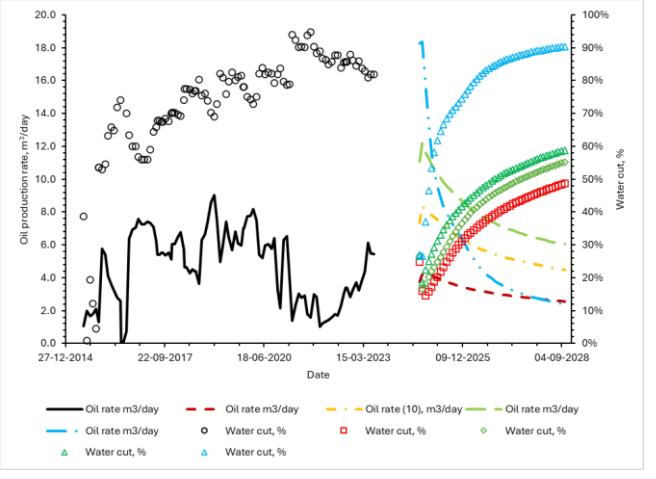

Fig. 9: Variations in oil production rate and water cut before and after the 15-month shut-in period, showing rapid stabilization of oil output and sustained reduction in water cut upon restart at the optimal rate of 15 m3·day⁻1.

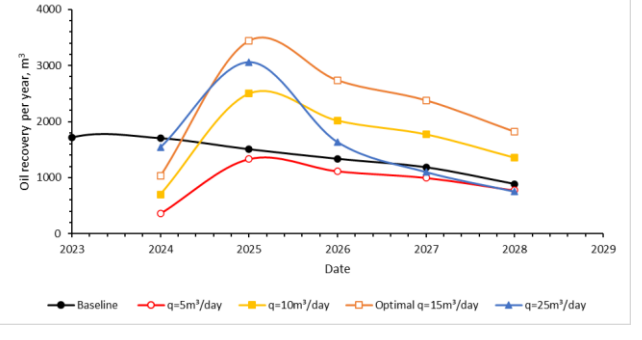

Fig. 10: Oil recovery per year versus time and flow rate (5–25 m3·day–1) after shut-in, compared to the baseline case.

3.3.3 Economic assessment of DFS approach for long-term high-WC well management

The results of the simulation were used to perform a brief economic assessment. Fig. 10 shows the annual oil production as a function of flow rate after shut-in and time, compared with the baseline case. As can be seen, restarting the well at a rate of 15 m^3·day^{-1} provides the highest incremental oil recovery relative to the baseline. The total oil production for the baseline case during June 2023 – October 2028 was 7,700 m^3, whereas the corresponding production obtained by restarting the well at 15 m^3·day^{-1} after a 15-month shut-in was 11,394 m^3, yielding an incremental oil volume of 3,694 m^3. Assuming an average oil price of 50 USD bbl^{-1}, this corresponds to an additional revenue of approximately 1,161,763 USD (considering that 1 m^3 ~6.29 bbl).

The cost of treating and disposing of water produced along with oil should not be neglected in the economic assessment. As can be perceived from Fig. 11, the simulation results demonstrated that, from June 2023 – October 2028, the baseline case generated up to 49,328 m^3 of unwanted produced water. In contrast, shutting in the well for 15 months and then restarting production at a rate of 15 m^3·day^{-1} resulted in only 9,733 m^3 of produced water. Water handling is already expensive, and in some cases, unit costs can reach US $2.5–5.0 per bbl.[48] This reduction in produced water volume offers

substantial savings in treatment and disposal costs. Assuming an average handling cost of US $3 per bbl, the optimized restart scenario reduces total water management expenses by about US $747,158 compared to the baseline.

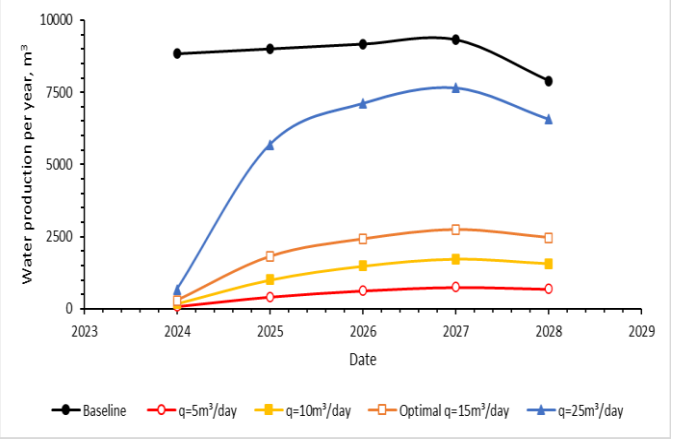

Fig. 11: Water production per year versus time and flow rate (5–25 $m^3 \cdot day^{-1}$) after shut-in, compared to the baseline case.

3.3.4 Partial-perforation analysis

To examine whether isolating part of the production interval could reduce water inflow, the effective perforation thickness was halved. As shown in Table 6, cumulative oil recovery decreased by 12–15 %, and production rate dropped by 18–22 % within the first day due to increased hydraulic resistance. The modification offered no economic advantage, as reduced oil output outweighed savings from lower water handling.

Table 6: Impact of reduced perforation thickness on four-year oil recovery.

Flow rate ($m^3 \cdot day^{-1}$)	Cumulative oil (m^3) – full interval	Cumulative oil (m^3) – half interval
5	4,584	4,048
10	8,349	6,410
15	11,394	6,535
25 (baseline)	8,088	6,535

3.3.5 Discussion and implications

The simulation results indicate that a restart rate of 15 $m^3 \cdot day^{-1}$ achieves the most favorable trade-off between oil recovery and water cut, increasing cumulative oil production by ~37 % relative to the 10 $m^3 \cdot day^{-1}$ case while maintaining manageable water handling. This regime also minimizes drawdown-induced instability and preserves segregated flow near the OWB. From a field-operations standpoint, the findings suggest that multi-month shut-ins are sufficient to enable gravity-driven re-segregation, after which controlled low-rate production can sustain oil output with minimal water entrainment. These insights provide quantitative guidelines for optimizing restart schedules in DFS applications.

To validate the simulation results against independent data, a comparison with literature results was conducted. For example, the study summarized by Carpenter (2015) reports the simulation of a cyclic-production scheme (CPS) as a method to control excessive water production in a mature oil field using a detailed reservoir-simulation model comprising 49 layers and approximately 3 million grid cells. In this approach, wells alternated between 8 months of production and 4 months of shut-in, during which gravity segregation allowed water to settle downward and oil to re-accumulate near the wellbore. The simulation results for 93 wells showed that CPS reduced water production by about 20% with only a slight reduction in oil output. The cyclic operation improved sweep efficiency through crossflow and streamline realignment and increased oil rates in adjacent offset wells. Overall, CPS proved to be an effective strategy for reducing water-handling costs and conserving reservoir energy in high-water-cut fields.

The following section presents field-scale validation of this workflow through pilot implementations conducted in Western Kazakhstan.

3.4 Pilot implementation in Western Kazakhstan

3.4.1 Field sites and reservoir characteristics

The developed DFS workflow was field-tested in three western Kazakhstan oilfields (Zhylankabak, Tamdykol, Karsak) to evaluate its performance under varied reservoir conditions and crude properties. These sites represent shallow, high-permeability formations typical of the region but with markedly different fluid characteristics. The most viscous oil occurs at Zhylankabak (~8,560 cP), while Tamdykol contains medium-viscosity crude (~80 cP), and Karsak exhibits moderately heavy oil (~775 cP). This diversity provided an opportunity to assess how gravitational segregation and controlled drawdown perform across distinct mobility ratios. The main reservoir and fluid parameters for each site are summarized in Table 7. All three formations exhibit high porosity–permeability systems conducive to rapid fluid segregation, and the broad viscosity range defines contrasting capillary–gravitational balances relevant to DFS application.

3.4.2 Field implementation and results

Table 8 shows the performance of the DFS workflow during pilot trials in the Zhylankabak, Tamdykol, and Karsak oilfields. In all cases, WC decreased by more than 90 %, while oil rates were either maintained or improved, confirming stable phase segregation and effective control of water inflow across a wide range of fluid properties.

Table 7: Reservoir and fluid parameters for the Zhylankabak, Tamdykol, and Karsak pilot sites*.

Parameter	Zhylankabak	Tamdykol	Karsak
Depth (m)	203–610	30–100	170–175
Reservoir temperature (°C)	23–28	20–25	25
Reservoir pressure (bar)	13–55	3–10	15
Permeability (mD)	800	910	1 657
Oil viscosity (cP)	8,560	80	775
Oil density ($g \cdot cm^{-3}$)	0.920	0.879	0.935
Brine density ($g \cdot cm^{-3}$)	1.033	1.080	1.090
Brine salinity (TDS, %)	4.7	15.0	13.4

Note*: All three formations are shallow and highly permeable, favoring rapid gravitational segregation. The wide viscosity range (80–8,560 cP) provided contrasting mobility regimes for assessing DFS performance.

Table 8: Pre- and post-implementation oil rates and water cuts for pilot wells in Western Kazakhstan*.

Parameter	Zhylankabak 54	Tamdykol 12	Tamdykol 5	Tamdykol 4	Karsak 1
Duration of pilot	1 month	3 months	3 months	3 months	3 months (ongoing)
Oil rate before ($t \cdot day^{-1}$)	1.0	0.3	0.1	0.1	0.4
Oil rate after ($t \cdot day^{-1}$)	1.0	1.8	1.1	0.5	0.35–0.40
Water cut before (%)	92	95	98	97	97
Water cut after (%)	< 0.5	< 1	< 1	< 1	< 1

Note*: DFS application lowered WC from 92–98 % to below 1 % while maintaining or increasing oil output in all wells.

Zhylankabak field

Well 54 at Zhylankabak contained extremely viscous oil (~8,560 cP) and initially produced about 1 $t \cdot day^{-1}$ (metric ton per day) of oil with WC 92 %. After one month of DFS operation, WC dropped to < 0.5 % while the oil rate remained unchanged. This outcome confirms that precise pump-intake placement above the stabilized OWB can sustain segregated flow even in low-mobility systems, validating the method's effectiveness under heavy-oil conditions.

Tamdykol field

Three Tamdykol wells were evaluated in a medium-viscosity regime (~80 cP). Before DFS installation, they produced 0.1–0.3 t·day–1 at WC = 95–98 %. After three months of continuous operation, oil rates increased several-fold, to 1.8, 1.1, and 0.5 t·day–1, while WC in all wells fell below 1 %. These results show that, where vertical permeability and reservoir connectivity are sufficient, gravity-driven segregation combined with controlled drawdown can simultaneously enhance oil mobility and suppress water encroachment, improving overall production efficiency.

Karsak field

The Karsak pilot (winter 2024–2025) involved moderately heavy crude (~775 cP) with a high pour point (~10 °C). Well 1, producing since 1963, initially yielded 0.4 $t \cdot day^{-1}$ at WC 97 %. Following shut-in and OWB identification (static 9 m; dynamic 12 m), a surface-mounted pump with electrical heating was installed to prevent paraffin deposition. Under this configuration, the well maintained 0.35–0.40 $t \cdot day^{-1}$ with WC < 1 %, demonstrating stable DFS performance under low-temperature, wax-prone conditions.

3.4.3 Comparative assessment

Across all pilots, DFS achieved consistent WC reduction to below 1 %, irrespective of crude viscosity, depth, or operating temperature. The Zhylankabak trial highlights DFS capability in highly viscous, low-mobility reservoirs; Tamdykol demonstrates the method's ability to improve both oil rate and fluid selectivity under moderate viscosities; and Karsak validates its adaptability in cold-flow, paraffinic systems. Together, these outcomes verify that gravitational segregation coupled with automated surface control provides a robust, chemical-free strategy for sustainable water-cut management. The field-scale findings presented here form the empirical basis for the analytical and numerical investigations discussed in the following section. The pilots were designed to assess operational feasibility and test the project's main hypothesis. Standard industry methods—water cut and oil flow rate measurements—were used, ensuring minimal uncertainty in the field data.

4. Limitations and directions for future research

The theoretical and laboratory work supporting this study was carried out under grant AP22787244, "Development of Innovative Well Production Technology for Enhancing Oil

Recovery, Reducing Operating Costs, and Carbon Footprint," in accordance with the approved plan. All costs for equipment fabrication and pilot testing were covered by the authors' personal funds.

The next phase should focus on designing and developing a certified, fully automated prototype that meets safety standards and incorporates advanced control systems for industrial use.

The combined experimental, analytical, and numerical results confirm that DFS can stabilize oil–water flow after shut-in and maintain low water cut under optimized restart conditions. However, the modeling assumes idealized boundaries, homogeneous rock, and stable interfaces. In practice, reservoir heterogeneity and fracture may affect the segregation and long-term performance, defining the technology's practical limits and guiding future improvements.

Overall, the presented work demonstrates the industrial applicability of DFS as a cost-effective and sustainable approach to improving oil recovery and reducing environmental impact in mature fields.

5. Conclusion

This research introduces and validates a novel oil production technology that leverages gravitational segregation within the wellbore to achieve selective oil extraction while suppressing water production.

Numerical simulations

Reservoir-scale modeling demonstrated that a 15-month well shut-in can lead to a significant redistribution of fluids in the near-wellbore zone. Oil saturation in the upper reservoir intervals increased from ~0.2–0.4 to 0.6, while the oil–water contact stabilized at ~1,541 m. Restarting production at 15 m^3/day was identified as the most favorable regime, maximizing cumulative oil recovery and limiting water cut, while higher restart rates triggered early water breakthrough. Overall economic benefit was estimated to be 3,694 m^3 of incremental oil recovery over 49 months.

Laboratory-scale validation

Experimental measurements confirmed that oil droplets with diameters between 5 and 20 mm are capable of rising through 250–500 m water columns within 1–16 hours, depending on viscosity (29–635 cP) and density (900–940 kg/m^3). These results support the fundamental feasibility of gravity-driven segregation and provide practical input parameters for modeling reservoir processes.

Analytical modeling

Theoretical analysis highlighted that gravitational rebalancing is highly sensitive to reservoir properties. Separation time grows linearly with formation thickness and increases exponentially with decreasing vertical permeability. For example, in a 13 m thick layer with a permeability of 0.4 Darcy, equilibrium was reached in approximately 193 days. This emphasizes the importance of screening candidate reservoirs based on permeability and thickness prior to field application.

Field-scale application

Pilot trials in high-water-cut wells (92–98%) provided practical confirmation of the method's effectiveness. The water cut was reduced to below 1%, even in heavy-oil reservoirs with viscosities as high as 8,560 cP. In fields with oil viscosity around 80 cP, production rates increased from 0.1–0.3 t/d to 0.5–1.8 t/d, demonstrating improvements in oil recovery.

General implications

Despite these positive outcomes, the method shows limitations in fractured or very low-permeability formations (<0.1 Darcy), where gravitational redistribution is too slow or unstable. In addition, its reliance on real-time automated monitoring and specialized surface equipment may pose economic challenges in mature, low-rate fields.

Future research should aim to:

- Define permeability thresholds that determine the applicability of the method.
- Advance automation and real-time monitoring technologies.
- Conduct multiwell pilot tests of the fully automated DFS prototype to validate its long-term performance, operational reliability, and scalability.

Acknowledgments

This work was carried out as part of the project "AP22787244 Development of Innovative Well Production Technology for Enhancing Oil Recovery, Reducing Operating Costs, and Carbon Footprint", funded by the Committee of Science of the Ministry of Science and Higher Education of the Republic of Kazakhstan.

Conflict of Interest

The authors have no conflict of interest to declare.

Supporting Information

Applicable.

Abbreviations

cP — Centipoise
CPS — Cyclic Production Scheme(s)
CSF — Continuum Surface Force (method)
DFS — Downhole Fluid Segregation
DWS — Downhole Water Sink
GDWS-AGD — Gas-Downhole Water Sink-Assisted Gravity Drainage
TC-GDWS-AGD — Triple-Completion Gas-Downhole Water

Sink-Assisted Gravity Drainage
DOWS — Downhole Oil–Water Separation
EOR — Enhanced Oil Recovery
ESP — Electric Submersible Pump
kh / kv — Horizontal/Vertical permeability
$m^3 \cdot day^{-1}$ — Cubic meters per day
mD — Millidarcy
MPa — Megapascal
OWB — Oil–Water Boundary
OWC — Oil–Water Contact
Re — Reynolds number
TDS — Total Dissolved Solids
WC — Water cut

CRediT Statement

Marat Sagyndikov: Conceptualization, Methodology, Writing – Original draft, Funding acquisition; **Iskander Gussenov:** Writing – Original draft, Writing – Review & editing; **Alexey Shakhvorostov:** Writing – Original draft, Writing – Review & editing; **Yerzhan Melis:** Writing – Original draft, Writing – Review & editing; **Ilshat Salimgarayev:** Formal analysis, Writing; **Batyrzhan Shilanbayev:** Simulation, Writing; **Reza Khoramian:** Simulation, Writing; **Zhalgas Imanbayev:** Conceptualization, Methodology.

References

[1] L. Xue, P. Liu, Y. Zhang, Status and prospect of improved oil recovery technology of high water cut reservoirs, *Water*, 2023, **15**, 1342, doi: 10.3390/w15071342.

[2] A. Rajbongshi, S. B. Gogoi, A review on oilfield produced water and its treatment technologies, *Petroleum Research*, 2024, **9**, 640-656, doi: 10.1016/j.ptlrs.2024.06.003.

[3] Y. Mao, Study on determination method of economic limit water cut of water drive oilfield in ultra-high water cut stage, *IOP Conference Series*: *Earth and Environmental Science*, 2020, **558**, 022059, doi: 10.1088/1755-1315/558/2/022059.

[4] D. Permana, F. Fakhrizal, M. P. Nurwibowo, Selection criteria for successful water shut-off treatment - brown field success story, *SPE Asia Pacific Oil and Gas Conference and Exhibition,* Jakarta, Indonesia, 2013, October 22-24, SPE-165753-MS., doi: 10.2118/165753-ms.

[5] Al-Muhanna, K., Habib, K., Experimental Study on the Effect of the Water-Cut Conditions on the Performance of L80 Carbon Steel, *Journal of Failure Analysis and Prevention*, 2013, **13**, 98–101, doi: 10.1007/s11668-012-9640-7.

[6] J. Sun, C. Sun, G. Zhang, W. Zhao, Y. Wang, Effect of water cut on the localized corrosion behavior of P110 tube steel in supercritical CO_2/oil/water environment, *Corrosion*, 2016, **72**, 1470-1482, doi: 10.5006/1926.

[7] C. de Waard, L. M. Smith, B. D. Craig, The influence of crude oils on well tubing corrosion rates, *CORROSION*, San Diego, 2003, March 16-21, 1-15, doi: 10.5006/c2003-03629.

[8] F. Seifi, F. Haghighat, H. Nikravesh, Y. Kazemzadeh, R. Azin, S. Osfouri, Using new chemical methods to control water production in oil reservoirs: comparison of mechanical and chemical methods, *Journal of Petroleum Exploration and Production Technology*, 2024, **14**, 2617-2655, doi: 10.1007/s13202-024-01844-1.

[9] Z. Alisheva, K. Nadirov, A. N. Al-Dujaili, G. Bimbetova, Z. Nadirova, M. Zhantasov, N. Tileuberdi, A. Dauletuly, Integrated strategies for controlling water cut in mature oil fields in Kazakhstan, *Polymers*, 2025, **17**, 829, doi: 10.3390/polym17070829.

[10] I. Gussenov, N. Nuraje, S. Kudaibergenov, Bulk gels for permeability reduction in fractured and matrix reservoirs, *Energy Reports*, 2019, **5**, 733-746, doi: 10.1016/j.egyr.2019.06.012.

[11] I. Gussenov, S. E. Kudaibergenov, Permeability reduction by gellan gum solutions, *Journal of Petroleum Science and Engineering*, 2022, **208**, 109546, doi: 10.1016/j.petrol.2021.109546.

[12] Shabibi M, Sahraei E., Identification of Water Production Mechanism in One of Iran's Oil Fields and Treat it with Gel Injection, *Journal of Chemical and Petroleum Engineering*, 2021, **55**(2), 223-242, doi: 10.22059/JCHPE.2021.312133.1334.

[13] P. Sharma, V. K. Kudapa, Study on the effect of cross-linked gel polymer on water shutoff in oil wellbores, *Materials Today*: *Proceedings*, 2022, **48**, 1103-1106, doi: 10.1016/j.matpr.2021.07.506.

[14] S. Hu, M. Ding, Y. Hu, Y. Wang, J. Dong, Optimization of the methods to develop stable polymer gels for water management in medium- and ultra-high-salinity reservoirs, *Gels*, 2023, **9**, 540, doi: 10.3390/gels9070540.

[15] Vargáné Árok, Z., Sáringer, S., Takács, D., Bretz, C., Juhász, Á., Szilagyi, I., Effect of salinity on solution properties of a partially hydrolyzed polyacrylamide, *Journal of Molecular Liquids*, 2023, **384**, 1-8, doi: 10.1016/j.molliq.2023.122192.

[16] C. M. Matthews, R. Chachula, B. R. Peachey, S. C. Solanki, Application of downhole oil/water separation systems in the alliance field, *SPE Health*, *Safety and Environment in Oil and Gas Exploration and Production Conference*, New Orleans, Louisiana, 1996, June 9-12, doi: 10.2118/35817-ms.

[17] B. R. Peachey, C. M. Matthews, Downhole oil/water separator development, *Journal of Canadian Petroleum Technology*, 1994, **33**(7), doi: 10.2118/94-07-01.

[18] Y. K. Bangash, M. Reyna, Downhole oil water separation (DOWS) systems in high-volume/high HP application, *SPE Latin American and Caribbean Petroleum Engineering Conference*, Port-of-Spain, Trinidad and Tobago, 2003, April 27-30, doi: 10.2118/81123-ms.

[19] C. Chapuis, Y. Lacourie, D. Lançois, Testing of down hole oil/water separation system in lacq superieur field, France, *SPE European Formation Damage Conference*, Hague, Netherlands, 1999, May 31-June 1, doi: 10.2118/54748-ms.

[20] C. Shaw, M. Fox, Economics of downhole oil-water separation: a case history and implications for the north sea, *European Petroleum Conference*, Hague, Netherlands, 1998, October 20-22, doi: 10.2118/50618-ms.

[21] Jiang, M., Cheng, T., Dong, K., Liu, J., Zhang, H., An Efficient Downhole Oil/Water-Separation System with Sucker-

Rod Pump, *SPE Production & Operations*, 2020, **35**, 522–536, doi: 10.2118/201234-PA.
[22] E. Sheridan, I. Ayling, J. Hixson, Downhole oil and water separation: a new start, *International Petroleum Technology Conference*, Beijing, China, 2013, March 26-28, doi: 10.2523/iptc-16914-abstract.
[23] John, A.V., Bruce, G.L., Stan, B., Feasibility evaluation of downhole oil/water separator (DOWS) technology, *UNT Digital Library*, 1999.
[24] Yang, G., He, L., Feng, L., Yong, Z., Bo, Y., Haoyu, L., Application of DOWS (Downhole Oil Water Separation) Technology Used in High Water-Cut Oilfield, *Oil & Gas Conference and Exhibition*, Asia Pacific, 2015, doi: 10.2118/176421-MS.
[25] Zaynullin, N.N., Improving the Efficiency of Low-Rate Well Operation and Designing Measures to Enhance Their Performance Using the Example of NGDU "Leninogorskneft" of PJSC "Tatneft", *Herald of Science*, **11**, 2023, 1–5.
[26] Kuzmichyov, N.G., Short-Term Operation of Wells for Viscous Oil Production Using ESPs, *Neftegaz*, 2015, **3**, 1–8.
[27] C. Wang, X. Zhang, R. Zhao, J. Shi, H. Zhao, Y. Sun, C. Xiong, F. Deng, Edge optimization analytics and control: a integrated device of intelligent intermittent pumping for tight oil wells, *Offshore Technology Conference Asia*, Kuala Lumpur, Malaysia, 2022, March 22-25, doi: 10.4043/31669-ms.
[28] S. Al-Mutairi, H. Al-Yousef, F. Al-Ajmi, H. Al-Hashim, Cyclic production scheme: innovative application in reducing water production and increasing ultimate recovery from mature areas, *SPE Saudi Arabia Section Technical Symposium*, Al-Khobar, Saudi Arabia, 2008, May 10-12, doi: 10.2118/120818-ms.
[29] Khuzin, R.R., Takhautdinov R.Sh., Shafigullin, M.G., Timirov V.S., Shayakhmetov A.Sh., Method for Producing Hard-to-Recover Oil Reserves, *E3S Web of Conferences*, 2003.
[30] A. K. Wojtanowicz, H. Xu, Z. Bassiouni, Oilwell coning control using dual completion with tailpipe water sink, *SPE Production Operations Symposium*, Oklahoma City, 1991, April 7-9, doi: 10.2118/21654-ms.
[31] A. K. Wojtanowicz, E. I. Shirman, H. Kurban, Downhole water sink (DWS) completion enchance OIL recovery in reservoirs with water coning problem, *SPE Annual Technical Conference and Exhibition*, Houston, Texas, 1999, October 3-6, doi: 10.2118/56721-ms.
[32] W. J. Al-Mudhafar, D. A. Al-Obaidi, D. Saini, A. K. Wojtanowicz, M. S. Al-Jawad, Feasibility of the gas and downhole water sink-assisted gravity drainage (GDWS-AGD) process to enhance the recovery of oil in reservoirs with strong aquifer, *Macromolecular Characterization of Hydrocarbons for Sustainable Future*, Singapore, 2021, 91-106, doi: 10.1007/978-981-33-6133-1_7.
[33] W. Al-Mudhafar, D. Wood, D. Al-Obaidi, A. Wojtanowicz, Well placement optimization through the triple-completion gas and downhole water sink-assisted gravity drainage (TC-GDWS-AGD) EOR process, *Energies*, 2023, **16**, 1790, doi: 10.3390/en16041790.
[34] W. J. Al-Mudhafar, D. A. Wood, Development and simulation of the gas-downhole water sink-assisted gravity drainage (GDWS-AGD) process to reduce carbon footprint and improve clean oil production by injecting CO_2 and petroleum-associated gas, *Journal of Cleaner Production*, 2024, **464**, 142792, doi: 10.1016/j.jclepro.2024.142792.
[35] R. A. Sadkhan, A. M. Almansor, W. J. Al-Mudhafar, K. Javid, D. N. Rao, Simulation of the triple completion-gas downhole water sink-assisted gravity drainage process through the re-injection of petroleum associated gas (PAG), *ADIPEC Exhibition and Conference*, Abu Dhabi, UAE, 2024, November 4-7, doi: 10.2118/222828-ms.
[36] M. Zeynolabedini, M. Assareh, Development of an effective design for a down-hole water sink to control water in oil production wells, *Cleaner Engineering and Technology*, 2021, **2**, 100072, doi: 10.1016/j.clet.2021.100072.
[37] T. Q. Nguyen, D. W. Green, G. P. Willhite, C. S. McCool, Effects of gelant composition and pressure gradients of water and oil on disproportionate permeability reduction of sandpacks treated with polyacrylamide-chromium acetate gels, *Society of Petroleum Journal*, 2006, **11**, 145-157, doi: 10.2118/89404-pa.
[38] Q.-H. Wu, J.-J. Ge, L. Ding, G.-C. Zhang, Unlocking the potentials of gel conformance for water shutoff in fractured reservoirs: Favorable attributes of the double network gel for enhancing oil recovery, *Petroleum Science*, 2023, **20**, 1005-1017, doi: 10.1016/j.petsci.2022.10.018.
[39] M. Varshney, A. Goyal, I. Goyal, A. Jain, N. Pandey, A. Parasher, S. Vermani, A. S. Negi, V. Sharma, Improving conformance in an injector well using delayed crosslink polymer gel: a case study, *SPE Asia Pacific Oil and Gas Conference and Exhibition,* Brisbane, Australia, 2018, October 23-25, doi: 10.2118/192136-ms.
[40] J. L. Scaramuzza, H. Fischetti, L. Strappa, S. Figliuolo, Downhole oil/water separation system – field pilot – secondary recovery application project, *SPE Latin American and Caribbean Petroleum Engineering Conference*, Buenos Aires, Argentina, 2001, March 25-28, doi: 10.2118/69408-ms.
[41] Varshney, M., Goyal, A., Goyal, I., Jain, A., Pandey, N., Parasher, A., Vermani, S., Negi, A.S., Sharma, V., Improving Conformance in an Injector Well Using Delayed Crosslink Polymer Gel, A Case Study, *Oil and Gas Conference and Exhibition*, Asia Pacific, 2018, doi: 10.2118/192136-MS.
[42] G. Ma, Y. Yu, R. Zhao, J. Shi, J. Wang, X. Zhang, S. Chen, G. Chen, Research on intelligent optimization of intermittent lift systems for low production oil wells, *International Petroleum Technology Conference*, Dhahran, Saudi Arabia, 2024, February 12, doi: 10.2523/iptc-24130-ms.
[43] Bakhtiy, N.S., Abdulina, M.V., Mokropulo, Yu.I., Equilibrium and Filtration of Oil and Water in a Porous Medium under the Influence of Capillary and Gravitational Forces, *Bulletin of Tyumen State University, Physical and Mathematical Modeling, Oil, Gas, Energy*, 2015, **1**, 102–111
[44] Ma, G., Yu, Y., Zhao, R., Shi, J., Wang, J., Zhang, X., Chen, S., Chen, G., Research on Intelligent Optimization of Intermittent Lift Systems for Low Production Oil Wells, *International*

Petroleum Technology Conference, 2024, doi: 10.2523/IPTC-24130-MS.
[45] Jafari, A., Pour, S.E.F., Gharibshahi, R., CFD simulation of biosurfactant flooding into a micromodel for enhancing the oil recovery, *International Journal of Chemical Engineering and Applications*, 2016, **7**(6), 353-358.
[46] R. Duman, Permian produced water: impact of rising handling costs and larger water cuts on wolfcamp growth, *Proceedings of the 7th Unconventional Resources Technology Conference*, Denver, Colorado, USA, 2019, July 22-24, doi: 10.15530/urtec-2019-401.
[47] I. Abdallah, Cost effective treatment of produced water using co-produced energy sources, *SPE Annual Technical Conference and Exhibition*, Amsterdam, Netherlands, 2014, October 27-29, doi: 10.2118/173475-stu.
[48] C. Carpenter, Cyclic-production-scheme performance evaluated using reservoir simulation, *Journal of Petroleum Technology*, 2013, **65**, 132-134, doi: 10.2118/1213-0132-jpt.